American Mineralogist, Volume 92, pages 1750–1755, 2007

Carbon is not required during crystallization to produce ferrobasalts/ferrodiorites (FTP rocks)

MATTHEW L. WHITAKER,* DONALD H. LINDSLEY, JAN M. KUBICEK WHITAKER, AND HANNA NEKVASIL

Department of Geosciences, Stony Brook University, Stony Brook, New York 11794-2100, U.S.A.

ABSTRACT

Experiments were conducted to determine whether the presence of graphite is required to produce the Fe-Ti-P-enrichment, silica-depletion trend seen in ferrobasalts and ferrodiorites/jotunites. A nominally anhydrous Snake River Plain olivine tholeiite was crystallized at 9.3 kbar in Fe-Pt capsules; the composition of the Fe-Pt alloy was empirically chosen such that the charge neither lost nor gained iron. The results of these experiments and those of previous experiments conducted in graphite are strikingly similar: in both cases the residual liquids were depleted in silica and enriched in Fe, Ti, and P. We conclude that the presence of carbon is *not* essential for producing this distinctive trend.

Keywords: Experimental petrology, tholeiite, crystal-liquid differentiation, phase equilibria

INTRODUCTION

Ferrobasalts found in the Craters of the Moon lava field in the Snake River Plain (SRP) and the ferrodiorites (jotunites) associated with massif anorthosites are remarkably similar in composition, and are characterized by a strong silica-depletion, Fe-Ti-P enrichment trend (FTP Rocks, Fig. 1: e.g., Frost and Frost 1997; Owens and Dymek 1992). Previous experimentalists successfully reproduced this trend by conducting crystallization experiments on a variety of tholeiitic starting compositions in graphite capsules with low bulk water contents at elevated pressures (~7–10 kbar, Litvin 2002; Scoates et al. 1999; Thompson 1975; Whitaker et al. 2007). Based on the use of graphite capsules in the reported experiments, an abundance of graphite within and near the Laramie Anorthosite Complex (LAC), and the experiments of Weidner (1982) showing that carbon greatly stabilizes liquids in the Fe-C-O system, Lindsley et al. (1999) proposed that carbon plays an essential chemical role in producing this trend.

Whitaker et al. (2007) showed that equilibrium crystallization of a single "dry" (0.05 wt% H_2O) olivine tholeiite melt (10.62 wt% MgO) at 9.3 kbar (~30 km depth) gave rise to residual liquids that followed the same compositional trend as the ferrobasalts of the Craters of the Moon lava field in the SRP and the ferrodiorites found in the LAC. However, because the experiments reported in Whitaker et al. (2007) were conducted in graphite capsules, there were no means of distinguishing the effect of pressure on the liquid evolution paths from the effect of graphite (and hence C-O species dissolved in the melt). We report here the results of a parallel set of experiments at 9.3 kbar in which almost all conditions were identical, except that the sample was isolated from carbon in these experiments.

EXPERIMENTAL METHODS

Experimental procedure

The starting material used here is the same nominally anhydrous olivine tholeiite (ICPP123-260, abbreviated I260) used in the experiments of Whitaker et al. (2007). Experiments in this study were conducted in Pt capsules that had been pre-soaked with Fe° foil to prevent net transfer of Fe between sample and capsule during the experiment. Fe-loss changes the bulk composition as well as f_{O_2} because the iron lost alloys with the capsule as metallic Fe°. The proper amount of Fe° foil used in the alloying process was determined iteratively with the goal that the sample should have neither gained nor lost Fe during the course of the experiment.

Capsules were cut from Pt tubing, and the bottoms crimped, welded, and flattened. A double-thickness of 0.0005" Fe metal foil was placed along the bottom of the capsule and around the inner diameter, leaving sufficient room at the top for welding. These capsules were then evacuated, dried, sealed in evacuated silica-glass ampoules, and alloyed at 1250 °C for 6 h prior to using in experiments. The Fe° foil was consumed in this process, becoming part of the capsule wall. The sample material was then loaded into the capsule up to the top of the Fe-alloyed portion of the capsule, and a disk of Pt-foil that had also been pre-alloyed with Fe as above was placed Fe-side down on top of the sample material.

The Fe-Pt capsule was crimped shut and dried by placing the loaded capsule into a silica glass tube with an Fe° oxygen "getter" and glass spacer to keep them separated. This assembly was evacuated and heated for 20 min in a vertical furnace with a drying geometry such that the capsule was heated to 800 °C while the Fe° "getter" was at ~600 °C, to prevent oxidation of the sample while drying. After cooling, the dried capsule was welded shut, the top flattened in a pellet press, and placed into a graphite outer sleeve to match as closely as possible the geometry of the cell assembly used in Whitaker et al. (2007). The cell assembly was then loaded into the ½" piston-cylinder apparatus and promptly pressurized to prevent re-adsorption of water. The bulk water content of a fused sample dried in this manner was found to be 0.05 wt% by micro-Fourier Transform Infrared Spectroscopy (FTIR).

Crystallization experiments were conducted using the piston-out method in which the pressure was slowly raised to a value approximately 2 kbar greater than the desired pressure of the experiment while still at room temperature; then the sample was heated to the melting temperature (1320 °C) before decreasing the overpressure. The sample remained at this melting temperature and pressure for 4 h to ensure complete fusion, then was rapidly cooled to the final crystallization temperature of the experiment, where the sample remained for 2–3 days. Each experiment was quenched by turning off the power, resulting in an initial cooling rate of ~100 °C/s.

Analytical techniques

The major element compositions of all phases in experimental run products were determined by electron microprobe. Alkali loss during microprobe analysis was minimized by analyzing for Na and K first and keeping the beam on a large raster size until just before the analysis began. The absence of normative corundum (Cor) in all residual glass compositions suggests minimal alkali loss. All pyroxene and olivine analyses were projected through QUILF (Andersen et al. 1993) and checked for equilibrium whenever the assemblage permitted.

* E-mail: matthewlwhitaker@aim.com

The IgPet Program Suite (Carr 2002) was used to conduct mass balance calculations using a least-squares routine as well as to calculate molar norms of all residual liquids and pyroxenes. The least-squares calculations (LSQ) yielded phase proportions (in wt%) and helped ensure that no major phases were overlooked during microprobe analysis. Only those combinations of phases in a single experiment that yielded sums of the squares of the residuals less than 0.15 are reported here (with one exception, noted later).

The water contents of select glasses were measured by analyzing doubly polished wafers of the experimental run products with micro-IR spectroscopy using the Nicolet 20SXB FTIR spectrometer and Spectra Tech IR Plan microscope at the American Museum of Natural History. Glass densities and total water concentrations were calculated via the methods of Dixon et al. (1995) and Mandeville et al. (2002).

RESULTS

Compositions of crystalline phases and residual glasses from all experiments are given in Table 1. Little to no compositional zoning was observed in the crystals with the exception of augite, which commonly displayed significant variation in non-quadrilateral components, especially Ti and Al. Only experiments that produced homogenous residual glass are reported here. Note that experiment I260-48, the first liquid listed, is 100% glass and reproduces the bulk composition of the I260 olivine tholeiite starting material. With the exception of the experiment conducted at 1260 °C, which lost ~0.6 wt% FeO (~6 relative% FeO), all bulk compositions as determined by LSQ are close to the FeO content of the starting material.

Figure 2a shows the computed abundances of phases present in the "dry" experiments on I260 in both graphite and Fe-Pt capsules. The phase abundances in the Fe-Pt experiments are similar to those found in the graphite experiments, save for a 20 °C offset in phase proportions and the lack of oxide phases in the Fe-Pt experiments.

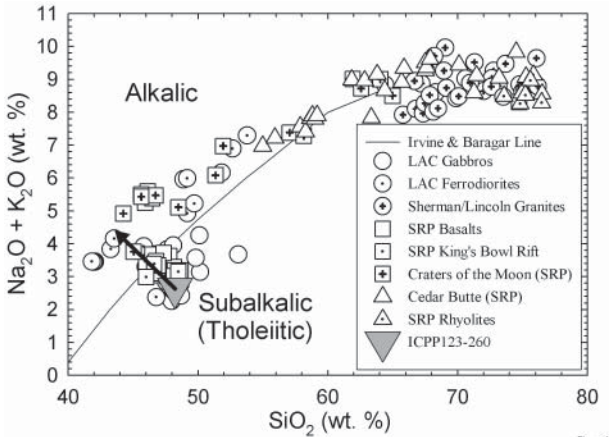

FIGURE 1. Total alkalis vs. silica variation in bulk compositions of natural rocks of the potassic silica-saturated alkalic trend (open symbols) from the Snake River Plain and non-cumulate rocks of the Laramie Anorthosite Complex (SRP basalts and basalts of the SRP King's Bowl Rift, Kuntz et al. 1992; basalts and intermediate rocks of Craters of the Moon lava field, Leeman et al. 1976; Stout and Nicholls 1977; Stout et al. 1994; intermediate rocks and rhyolites of Cedar Butte, McCurry et al. 2007; SRP rhyolites, Leeman 1982; LAC gabbros, Mitchell et al. 1995; LAC ferrodiorites, Mitchell et al. 1996; Sherman/Lincoln granites, Frost et al. 1999). The Irvine and Baragar line separates the alkalic and sub-alkalic fields (Irvine and Baragar 1971). All data presented here and in subsequent variation diagrams are normalized to 100% volatile-free. ICPP123-260 (dark gray triangle) olivine tholeiite is the starting material used in this study. Arrow shows silica-depletion trend from 9.3 kbar experiments of Whitaker et al. (2007).

Figure 2b shows olivine and pyroxene compositions as projected through QUILF (Andersen et al. 1993) via the method of Lindsley and Andersen (1983, pages A894–A895). The open symbols are pyroxenes and olivines from the graphite experiments of Whitaker et al. (2007). The compositions of these phases follow the same trends in both sets of experiments.

The compositional relationships between feldspars and liquids are shown in Figure 2c. The molar normative feldspar components (An, Ab, Or) of the residual liquids, feldspars, and pyroxenes (included in this projection for mass balance) were normalized to 1. Results of the graphite experiments are shown as open symbols for comparison.

As was observed in the experiments conducted in graphite, residual liquids produced at 9.3 kbar in Fe-Pt capsules become strongly depleted in silica and enriched in total alkalis, crossing the boundary into the alkalic field (Fig. 2d). The strong silica-depletion of the residual liquids is accompanied by depletion in MgO and CaO, and strong enrichment in FeO_T, TiO_2, and P_2O_5 (Fig. 3). The residual liquids from the experiments conducted in graphite are shown as gray circles for comparison.

DISCUSSION

The results of these experiments show good agreement with the experiments conducted in graphite capsules in both mineral phase and residual liquid compositions. One difference between the two sets of experiments is that the graphite-free experiments consistently yielded an assemblage equivalent to that seen 20 °C higher in the graphite capsule experiments (Fig. 2a). This may have arisen from two factors. First, during the melting period of each graphite experiment, a "drift" in the temperature reading of ~4 °C had been noted at the melting temperature during the 2 h melting period. This may be the result of minor diffusion of Rh into the pure Pt leg of the thermocouple. It is likely that this drift in temperature is greater in the graphite-free experiments because of the necessary 4 h melting period. This drift causes the temperature read by the controller to be lower than the actual temperature of the experiment. Second, although the rest of the cell assembly was identical, the details in the vicinity of the capsule were necessarily slightly different, which may have produced a slightly different temperature gradient across the cell.

Two differences were noted between the assemblages crystallizing in the graphite experiments and those crystallizing in Fe-Pt. One was the absence of oxide phases in the latter. This may have been caused by a slight difference in f_{O_2}. A net loss of Fe to the capsule, as occurred in the highest temperature experiment, would cause the f_{O_2} to be somewhat higher, because the ferric/ferrous ratio of the charge goes up. Similarly, f_{O_2} would be lower if there was a net gain of Fe from the capsule. However, with the exception of the 1260 °C experiment, the least-squares calculations for all other experiments indicate that the capsule is truly "neutral" with respect to Fe loss or gain; therefore the f_{O_2} should have been the same as that of the starting material. In addition, the QUILF projections of the augites in the Fe-Pt experiments do not indicate any Fe^{3+}, which would be expected if the

sample lost Fe° to the capsule, further supporting the capsule's neutrality with respect to Fe content. The close similarity of phase compositions between these experiments and those conducted in graphite suggests that neither set of experiments underwent any significant oxidation or reduction with respect to the other, indicating that the f_{O_2} in both sets of experiments was also similar (~2.5 log units below FMQ, Whitaker et al. 2007). It is thus more likely that since the oxides are volumetrically minor phases, they may have been present but not observed in thin section.

A second difference between the experimental phase assemblages produced in these two sets of experiments is that the olivine in the highest temperature experiment in Fe-Pt is more magnesian than that found in the highest temperature graphite experiment (Fig. 2b). This may be the result of some Fe loss to the capsule during high-temperature crystallization. Perhaps this explains the results of the least-squares mass balance calculations for this experiment (1260 °C), which showed greater residuals compared to the rest (see Table 1). Experiments conducted at lower temperatures show a much closer match in ferromagnesian mineral compositions between the experiments conducted in Fe-Pt and graphite. The feldspars crystallizing in Fe-Pt are nearly identical in composition to those crystallizing in graphite (Fig. 2c).

The residual liquid compositions follow similar evolutionary paths in the Fe-Pt and graphite experiments (Figs. 2d and 3). Both sets of experiments lead to the strong silica-depletion, Fe-Ti-P-enrichment trend observed in ferrobasalts from the Craters of the Moon in the Snake River Plain and the ferrodiorites of the Laramie Anorthosite Complex. However, there are some differences. The most striking difference in liquid compositions between the two sets of experiments is found in Na_2O, which is consistently lower in Fe-Pt than in graphite. It is possible that some of the Na in the sample was lost to the Fe-Pt capsule during the experiment to form NaPt, and went statistically undetected in the least-squares calculations.

Since the Fe-Pt capsule was held by a graphite sleeve in the experiments, the run products were analyzed by FTIR to check for the presence of any C-O species that might have diffused in through the capsule wall. While the spectrum indicated some C-O dissolved in the residual glass (ppm range), it was only slightly more than the amount observed in experiments conducted in the absence of graphite, and 3 or more orders of magnitude less than

Table 1. Representative residual liquid and mineral phase compositions (in wt%) from "Dry" I260 experiments in Fe-Pt at 9.3 kbar

Phase	**Liquid**	**Liquid**	Olivine	**Liquid**	Olivine	Augite	**Liquid**	Olivine	Augite	Plag	**Liquid**
Experiment (No.)	**I260-48**	**I260-226**	I260-226	**I260-223**	I260-223	I260-223	**I260-187**	I260-187	I260-187	I260-187	**I260-189**
T (°C)	**1320**	**1260**	1260	**1240**	1240	1240	**1200**	1200	1200	1200	**1180**
SiO_2	47.53	47.78	40.43	47.61	39.24	50.07	45.32	37.30	48.99	52.32	44.42
TiO_2	1.43	1.47	0.03	1.67	0.03	0.71	2.59	0.02	1.08	0.07	3.41
Al_2O_3	15.03	15.37	0.15	16.39	0.09	8.03	15.76	0.07	7.52	29.31	14.82
FeO	10.53	10.04	14.09	10.74	18.01	7.93	12.61	23.89	9.26	0.31	15.08
MnO	0.16	0.15	0.16	0.19	0.21	0.21	0.20	0.20	0.20	0.00	0.19
MgO	10.46	10.43	45.64	8.46	41.89	17.59	6.78	36.59	16.20	0.14	5.65
CaO	10.57	10.80	0.35	10.35	0.38	13.81	9.44	0.29	14.48	12.54	8.94
Na_2O	2.18	2.38	0.01	2.53	0.03	0.42	2.68	0.01	0.52	4.14	2.84
K_2O	0.42	0.45	0.01	0.54	0.01	0.00	0.78	0.01	0.00	0.29	1.10
P_2O_5	0.26	0.39	0.16	0.43	0.04	0.18	0.46	0.04	0.03	0.03	0.86
Total	98.57	99.25	101.03	98.91	99.94	98.94	96.61	98.42	98.29	99.16	97.31
Comp. (mol%)	–	–	Fo85(La0.5)	–	Fo80(La0.5)	En64Wo20	–	Fo73(La0.4)	En58Wo23	An62(Or2)	–
Abundance (wt%)	100.0	99.4	0.6	84.3	2.5	13.2	47.2	8.6	24.9	19.3	25.3
Mg no.*	0.68	0.68	–	0.62	–	–	0.53	–	–	–	0.44
H_2O (wt%)	0.05†	0.05†	–	0.06†	–	–	0.11†	–	–	–	0.20‡
S.S.R.§	N/A	0.37		0.04			0.02				0.05

Phase	Olivine	Augite	Plag	**Liquid**	Olivine	Augite	Plag	**Liquid**	Olivine	Augite	Plag
Experiment (No.)	I260-189	I260-189	I260-189	**I260-192**	I260-192	I260-192	I260-192	**I260-229**	I260-229	I260-229	I260-229
T (°C)	1180	1180	1180	**1160**	1160	1160	1160	**1140**	1140	1140	1140
SiO_2	36.66	47.99	52.63	43.19	36.74	47.91	53.34	42.36	36.82	48.06	54.72
TiO_2	0.07	1.22	0.08	4.27	0.06	1.59	0.10	5.63	0.07	2.00	0.12
Al_2O_3	0.12	7.60	28.96	14.52	0.13	7.77	29.14	14.09	0.15	7.90	28.44
FeO	27.20	10.03	0.38	15.63	29.24	11.17	0.39	16.55	30.57	11.54	0.49
MnO	0.31	0.25	0.04	0.24	0.32	0.22	0.00	0.28	0.36	0.25	0.00
MgO	33.87	14.86	0.04	5.51	32.08	14.36	0.09	3.68	31.71	14.13	0.12
CaO	0.35	15.00	11.66	8.60	0.33	14.86	11.43	8.21	0.34	14.77	11.12
Na_2O	0.02	0.53	4.41	2.68	0.06	0.50	4.53	2.57	0.02	0.50	4.72
K_2O	0.01	0.01	0.45	1.22	0.01	0.00	0.52	1.70	0.00	0.01	0.76
P_2O_5	0.14	0.03	0.00	0.97	0.20	0.05	0.08	1.60	0.13	0.21	0.20
Total	98.74	97.52	98.66	96.83	99.16	98.42	99.61	96.66	100.17	99.36	100.67
Comp. (mol%)	Fo69(La0.5)	En55Wo25	An58(Or3)	–	Fo66(La0.5)	En53Wo25	An56(Or3)	–	Fo65(La0.5)	En51Wo25	An54(Or4)
Abundance (wt%)	12.7	31.1	30.9	15.6	13.9	35.5	35.0	8.9	14.9	38.4	37.8
Mg no.*	–	–	–	0.42	–	–	–	0.32	–	–	–
H_2O (wt%)	–	–	–	0.32‡	–	–	–	0.56‡	–	–	–
S.S.R.§				0.05				0.04			

Note: Column headings in bold indicate liquid, as opposed to crystalline, phase analyses.
* Mg no. = Molar Mg/(Mg + Fe^{2+}) assuming an Fe^{2+}/Fe_T ratio of 0.85.
† Measured by FTIR.
‡ Calculated based on bulk water content and degree of crystallinity.
§ S.S.R. = Sum of squared residuals.

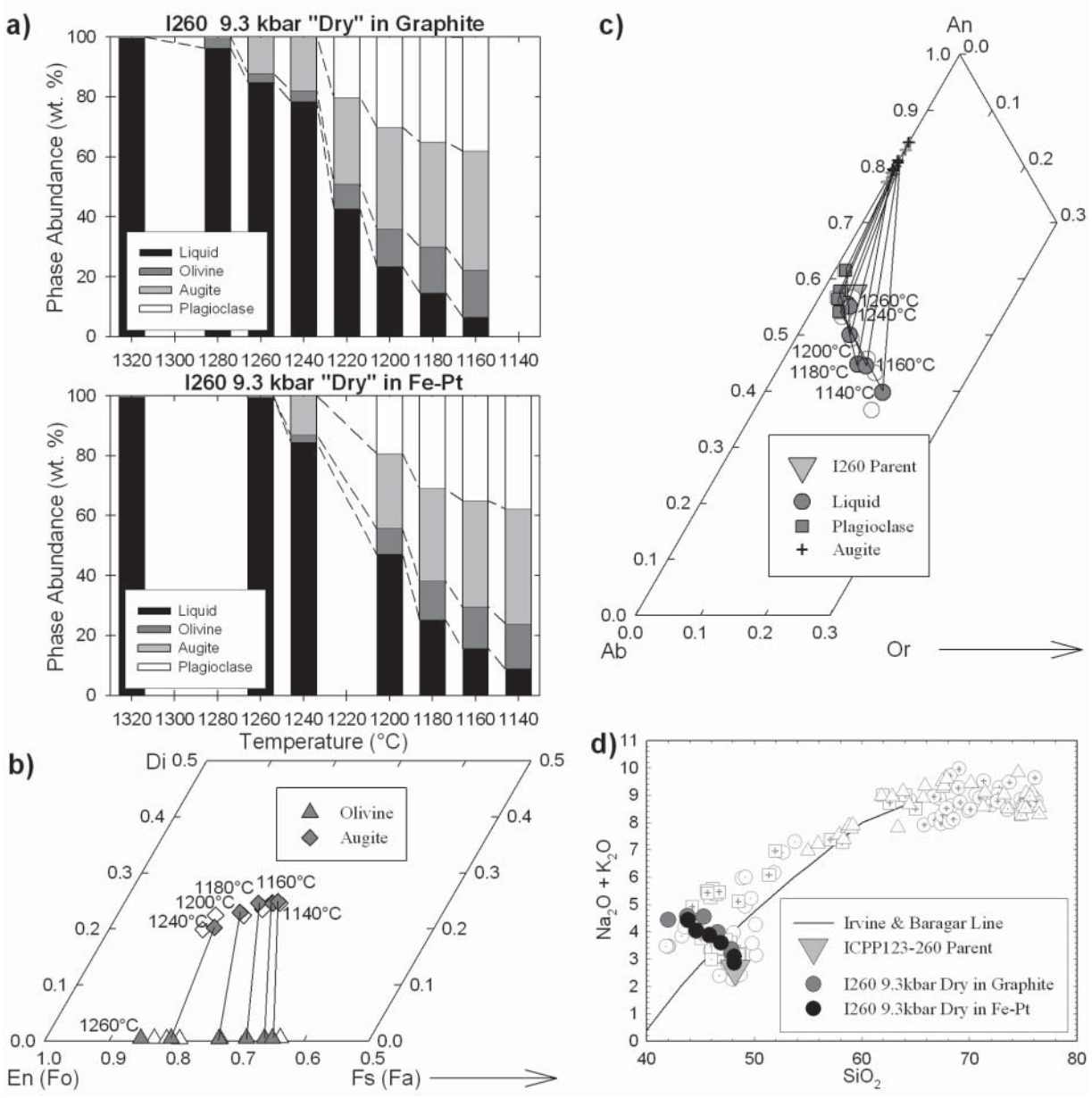

FIGURE 2. (**a**) Variation in phase abundances (wt%) with temperature of "dry" experimental run products of I260 in graphite (upper) and Fe-Pt (lower) capsules. Trace spinel present in graphite from 1200–1180 °C; 0.2 wt% ilmenite present in graphite at 1160 °C. Oxide phases not found in Fe-Pt experiments. (**b**) QUILF projections of olivine (gray triangles) and pyroxene (gray diamonds) compositions from "dry" experimental run products of I260 in Fe-Pt capsules. (**c**) Plagioclase compositions (gray squares) and molar normative feldspar constituents of glass (gray circles) and pyroxene (black crosses) of I260 "dry" experiments in Fe-Pt capsules. (**b** and **c**) Gray symbols are phase compositions from experiments in graphite. Tie lines connect coexisting phases. Temperatures of experiments are shown. (**d**) Total alkalis vs. silica variation of "dry" experiments on I260 at 9.3 kbar in graphite (gray circles) and Fe-Pt (black circles) capsules. Other symbols as in Figure 1.

that dissolved in the glasses from experiments run in graphite (wt% range). An experiment was also re-run using the same conditions, but with a crushable alumina sleeve surrounding the Fe-Pt capsule to remove any possibility of C entering the run, and the results of that experiment still showed the silica-depletion, Fe-Ti-P-enrichment trend of our other experiments.

The results of the experiments conducted in this study show good agreement with those conducted at 9.3 kbar in graphite by Whitaker et al. (2007). The liquids and crystalline assemblages from both sets of experiments follow similar evolutionary paths, resulting in the production of ferrobasaltic/ferrodioritic characteristics in the residual liquids (FTP rocks). These results suggest

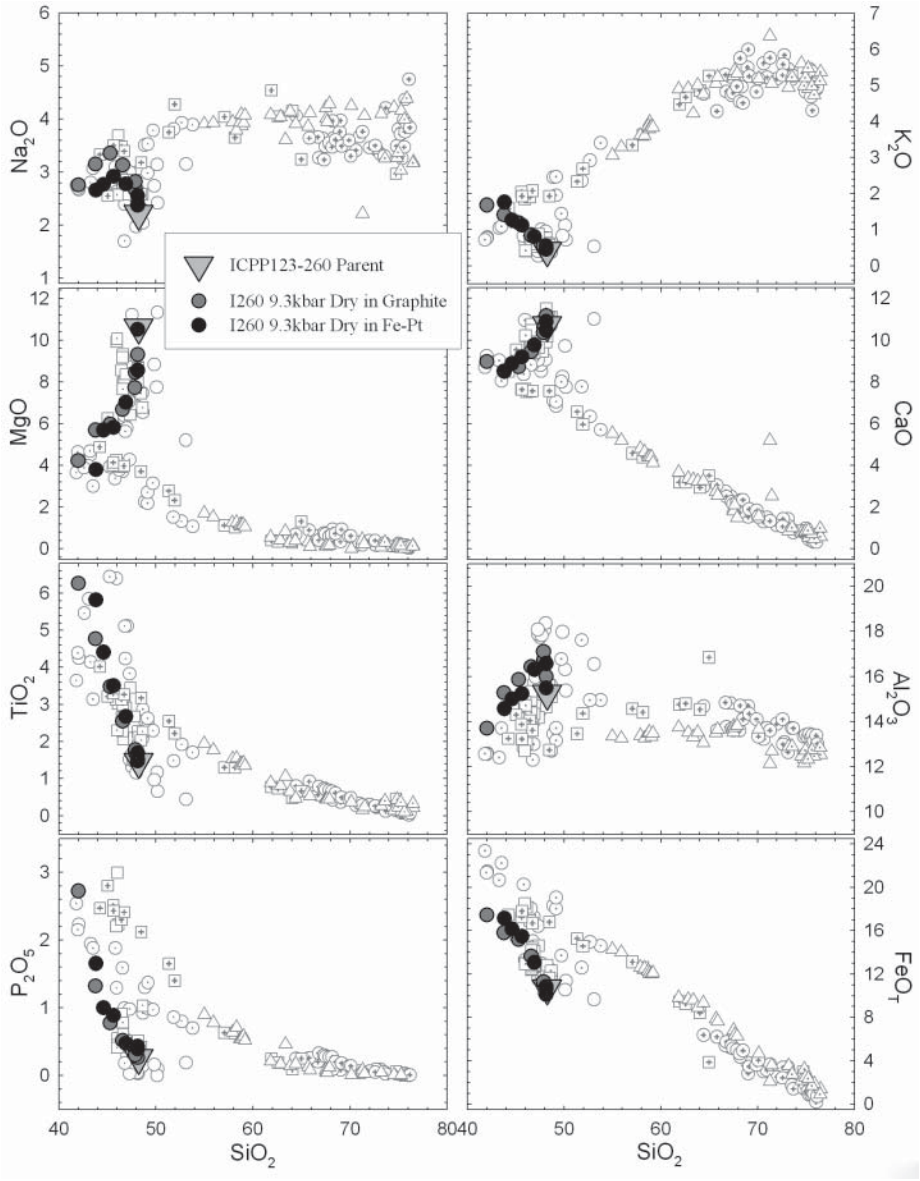

FIGURE 3. Major element Harker variation diagrams of residual liquid compositions (wt%) of experiments on "dry" I260 (gray triangle) at 9.3 kbar in graphite (gray circles) and Fe-Pt (black circles) capsules. Other symbols are as in Figure 1.

that, despite the natural association of graphite with ferrodiorites in anorthosite complexes, the presence of C-O species in the melt during crystallization is not necessary to generate liquids of the silica-depletion, Fe-Ti-P-enrichment trend.

ACKNOWLEDGMENTS

The authors gratefully acknowledge H.R. Naslund and J. Longhi, whose helpful and constructive reviews helped to improve this manuscript, and the financial support of NSF grant EAR 0003443 to D.H.L. and H.N., and a summer REU extension of this grant for J.M.W.

REFERENCES CITED

Andersen, D.J., Lindsley, D.H., and Davidson, P.M. (1993) QUILF—a Pascal program to assess equilibria among Fe-Mg-Mn-Ti oxides, pyroxenes, olivine, and quartz. Computers and Geosciences, 19(9), 1333–1350.

Carr, M.J. (2002) IgPet for Windows. Terra Softa Inc., Somerset, New Jersey.

Dixon, J.E., Stolper, E.M., and Holloway, J.R. (1995) An experimental study of water and carbon dioxide solubilities in mid-ocean ridge basaltic liquids Part 1: Calibration and solubility models. Journal of Petrology, 36(6), 1607–1631.

Frost, C.D. and Frost, B.R. (1997) Reduced rapakivi-type granites: The tholeiite connection. Geology, 25(7), 647–650.

Frost, C.D., Frost, B.R., Chamberlain, K.R., and Edwards, B.R. (1999) Petrogenesis of the 1.43 Ga Sherman batholith, SE Wyoming, USA: A reduced, rapakivi-type anorogenic granite. Journal of Petrology, 40(12), 1771–1802.

Irvine, T.N. and Baragar, W.R.A. (1971) Guide to chemical classification of common volcanic rocks. Canadian Journal of Earth Sciences, 8(5), 523–548.

Kuntz, M.A., Covington, H.R., and Schorr, L.J. (1992) An overview of basaltic volcanism of the eastern Snake River plain, Idaho. In P.K. Link, M.A. Kuntz, and L.B. Platt, Eds., Regional geology of eastern Idaho and western Wyoming, 179, p. 227–267. Geological Society of America Memoir, Boulder, Colorado.

Leeman, W.P. (1982) Rhyolites of the Snake River Plain—Yellowstone Plateau province, Idaho and Wyoming; A summary of petrogenetic models. In B. Bonnichsen, and R.M. Breckenridge, Eds., Cenozoic Geology of Idaho: Bulletin, 26, p. 203–212. Idaho Bureau of Mines and Geology, Moscow, Idaho.

Leeman, W.P., Vitaliano, C.J., and Prinz, M. (1976) Evolved lavas from the Snake River Plain—Craters of the Moon National Monument, Idaho. Contributions to Mineralogy and Petrology, 56(1), 35–60.

Lindsley, D.H. and Andersen, D.J. (1983) A two-pyroxene thermometer. Journal of Geophysical Research, 88, A887–A906.

Lindsley, D.H., Nekvasil, H., Scoates, J.S., and Dondolini, A. (1999) Dissolved carbon: A possible answer to the enigma of Fe-enriched magmas. EOS (Transactions, American Geophysical Union), 80(17), S367.

Litvin, V.Y. (2002) Application of fractional crystallization to the origin of continental tholeiitic suites, p. x–138. M.S. thesis, Department of Geosciences, State University of New York at Stony Brook, U.S.A.

Mandeville, C.W., Webster, J.D., Rutherford, M.J., Taylor, B.E., Timbal, A., and Faure, K. (2002) Determination of molar absorptivities for infrared absorption bands of H_2O in andesitic glasses. American Mineralogist, 87(7), 813–821.

McCurry, M., Hayden, K.P., Morse, L.H., and Mertzman, S. (2007) Genesis of post-hotspot A-type rhyolite of the Eastern Snake River Plain volcanic field by extreme fractional crystallization of olivine tholeiite. Bulletin of Volcanology, in press, DOI: 10.1007/s00445-007-0143-4.

Mitchell, J.N., Scoates, J.S., and Frost, C.D. (1995) High-Al gabbros in the Laramie Anorthosite Complex, Wyoming—Implications for the composition of melts parental to Proterozoic anorthosite. Contributions to Mineralogy and Petrology, 119, 166–180.

Mitchell, J.N., Scoates, J.S., Frost, C.D., and Kolker, A. (1996) The geochemical evolution of anorthosite residual magmas in the Laramie Anorthosite Complex, Wyoming. Journal of Petrology, 37, 637–660.

Owens, B.E. and Dymek, R.F. (1992) Fe-Ti-P-Rich Rocks and Massif Anorthosite—Problems of Interpretation Illustrated from the Labrieville and St-Urbain-Plutons, Quebec. Canadian Mineralogist, 30, 163–190.

Scoates, J.S., Lindsley, D.H., van der Kolk, D., and Anderson, K. (1999) Fractional crystallization experiments on a candidate parental magma to anorthosite. EOS (Transactions, American Geophysical Union), 80(46, Suppl.), F1096.

Stout, M.Z. and Nicholls, J. (1977) Mineralogy and petrology of Quaternary lavas from the Snake River Plain, Idaho. Canadian Journal of Earth Sciences, 14, 2140–2156.

Stout, M.Z., Nicholls, J., and Kuntz, M.A. (1994) Petrological and mineralogical variations in 2500–2000 yr B.P. lava flows, Craters of the Moon lava field, Idaho. Journal of Petrology, 35, 1681–1715.

Thompson, R.N. (1975) Primary basalts and magma genesis II. Snake River Plain, Idaho, USA. Contributions to Mineralogy and Petrology, 52, 213–232.

Weidner, J.R. (1982) Iron-oxide magmas in the system Fe-C-O. Canadian Mineralogist, 20, 555–566.

Whitaker, M.L., Nekvasil, H., Lindsley, D.H., and DiFrancesco, N.J. (2007) The role of pressure in producing compositional diversity in intraplate basaltic magmas. Journal of Petrology, 48, 365–393.

Manuscript received March 19, 2007
Manuscript accepted May 21, 2007
Manuscript handled by Bryan Chakoumakos